



Mobile platform center shift in spherical parallel manipulators with flexible limbs



Guanglei Wu, Shaoping Bai^{*}, Jørgen Kepler

Department of Mechanical and Manufacturing Engineering, Aalborg University, DK-9220 Aalborg, Denmark

ARTICLE INFO

Article history:

Received 2 July 2013

Received in revised form 30 December 2013

Accepted 5 January 2014

Available online xxxx

Keywords:

Spherical parallel manipulator

MP center shift

Virtual-spring method

Cartesian stiffness matrix

ABSTRACT

Spherical parallel manipulators (SPMs) with revolute joints work under the condition that all joint axes intersect at the manipulator center, where the mobile platform (MP) center is coincident with the center of the base platform. The center of each platform is the point of concurrence of the axes of the three revolute joints attached to the platform. When limb flexibility is considered, however, the MP center will shift away from the base platform center, which consequently influences the manipulator performance, e.g., its orientation accuracy. In this work, the stiffness of SPMs is analyzed, with focus on the MP center shift. The stiffness is modeled by adopting the virtual-spring method. Castigliano's theorem is used to calculate the limb deflection. The model is validated via FE analysis. Examples are included to show the center shift of SPMs with different designs.

© 2014 Elsevier Ltd. All rights reserved.

1. Introduction

A fundamental assumption for spherical parallel manipulators (SPMs) is that all links of the manipulator rotate about the manipulator center [1], i.e., the point of concurrency of the axes of all nine revolute joints. This assumption is valid for rigid-body motion or manipulators consisting of a ball-and-socket joint as the center of rotation. However, in the presence of link flexibility, the axes of all joints may not intersect at one common point. In other words, the center of the mobile platform (MP) will shift away from the center of the base platform. As this shift will consequently influence the performance of the manipulator orientation accuracy, it is important to investigate this shift from a design perspective.

The center shift in question is the result of limb deformation, which can be quantified based on stiffness analysis. Of the existing methods of stiffness modeling, the Virtual Joint Method (VJM), which is often called lumped modeling, has been widely used to establish the stiffness model for parallel manipulators (PMs), as it provides acceptable accuracy in short computational time. Gosselin first applied this approach to parallel manipulators [2], in which only actuator compliance was taken into account under an unloaded equilibrium condition. Chen and Kao proposed the Conservative Congruence Transformation (CCT) [3] to analyze the influence of changes of the robot geometry on the manipulator stiffness due to an external wrench. In general, link flexibility was considered in the stiffness modeling. In Gosselin and Zhang's work [4], the flexible links were replaced with rigid beams mounted on revolute joints supplied with torsional springs. This flexible-link, lumped-parameter model was also used by Majou et al. [5] to characterize the stiffness of the Orthoglide robot. Quennouelle and Gosselin considered the influence of the passive joints during stiffness modeling [6]. Combining the advantages of the existing methods, a systematic virtual-spring method was proposed to analyze translational parallel manipulators [7], which considers the link deflection and the influence of the passive joints simultaneously. The difference among the various VJM approaches lies in both the modeling assumptions and the numerical techniques. The stiffness of different types of PMs has been extensively investigated, whereas the stiffness modeling and analysis of this class of SPM have received less attention. Liu et al. [8] developed a stiffness model based on

^{*} Corresponding author. Tel.: +45 9940 9291; fax: +45 9940 7110.

E-mail addresses: gwu@m-tech.aau.dk (G. Wu), shb@m-tech.aau.dk (S. Bai), jk@m-tech.aau.dk (J. Kepler).

Gosselin's work [2], in which only the actuation compliance is considered. Recently, the stiffness analysis of a 3-RRP SPM was conducted on the basis of strain energy and Castigliano's theorem, while ignoring the influence of the passive joints and strain energy due to shear forces [9]. As SPMs are widely used as orientating devices, the previous stiffness analyses were limited to investigate the orientational deformation. However, the translational deformation of SPMs is an important consideration [10]. It is known that in the VJM approach, the Cartesian stiffness matrix relies on the calculation of both the mechanism Jacobian and stiffness matrices in joint space. When applying the virtual spring method to SPMs, one challenge is the computational burden of the complicated kinematics problem due to the products of trigonometric functions, since the inverse-kinematics solutions of all the limbs are to be solved in advance, to derive the Jacobian, as in Pashkevich's approach [7]. Thus, a simple and fast procedure is needed for modeling the stiffness of SPMs to investigate both the position and orientation accuracies.

In this paper, the MP center shift of spherical parallel manipulators is studied. A method to model the stiffness of SPMs for the analysis of the shift is developed and validated through FE analysis. We adopted the virtual-spring method in connection with Castigliano's theorem to calculate the limb stiffness in SPMs. Examples are included to illustrate the application of the method.

2. Problem formulation

A general spherical parallel manipulator is shown in Fig. 1. The i th limb consists of three revolute joints, whose axes are parallel to the unit vectors \mathbf{u}_i , \mathbf{v}_i , and \mathbf{w}_i . All three limbs have identical architectures, defined by angles α_1 and α_2 . Moreover, β and γ define the geometry of two triangular pyramids on the base and the mobile platforms, respectively. The origin O of the base coordinate system xyz is located at point O . The z axis is normal to the bottom surface of the base pyramid and points upwards, while the y axis is located in the plane made by the z -axis and \mathbf{u}_1 .

Under rigid-body motion, all the joint axes intersect at one point, namely, point O in Fig. 2(a). In a real-life system the manipulator will deform when subjected to external loads. Assuming that both the MP and the base platform are rigid, while the limb links are linearly elastic, the SPM will have two centers, one on the base platform, and one on the MP, which is movable, as illustrated in Fig. 2(b). The modeling of the shift of the MP center and the associated orientation error are the main issues studied here.

3. Error modeling of SPMs

Under the prescribed coordinate system, unit vector \mathbf{u}_i is derived as

$$\mathbf{u}_i = [-\sin\eta_i \sin\gamma \quad \cos\eta_i \sin\gamma \quad -\cos\gamma]^T \quad (1)$$

where $\eta_i = 2(i - 1)\pi/3$, $i = 1, 2, 3$.

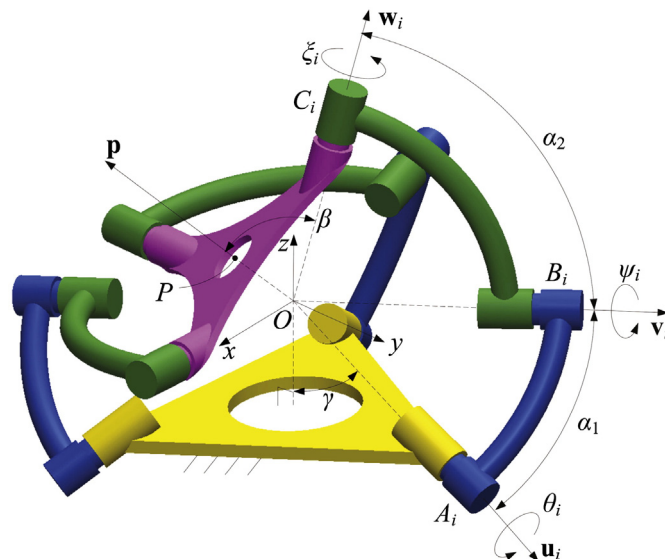


Fig. 1. Architecture of a general SPM.

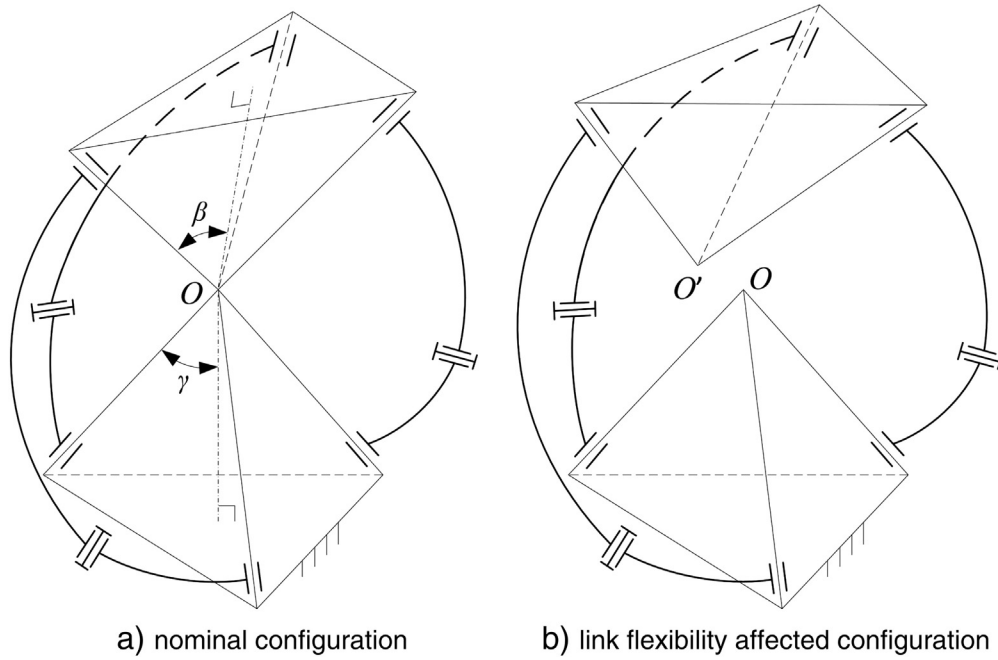


Fig. 2. Center separation of a SPM under an external wrench due to link flexibility.

The unit vector \mathbf{v}_i of the axis of the intermediate revolute joint in the i th leg is expressed as:

$$\mathbf{v}_i = \begin{bmatrix} -s\eta_i s\gamma c\alpha_1 + (c\eta_i s\theta_i - s\eta_i c\gamma c\theta_i) s\alpha_1 \\ c\eta_i s\gamma c\alpha_1 + (s\eta_i s\theta_i + c\eta_i c\gamma c\theta_i) s\alpha_1 \\ -c\gamma c\alpha_1 + s\gamma c\theta_i s\alpha_1 \end{bmatrix} \quad (2)$$

The unit vector \mathbf{w}_i of the top revolute joint in the i th leg is a function of the orientation of the mobile platform, namely,

$$\mathbf{w}_i = [w_{ix} \ w_{iy} \ w_{iz}]^T = \mathbf{Q}\mathbf{w}_i^* \quad (3)$$

where \mathbf{Q} is the rotation matrix that carries the MP from its reference orientation to the current one and \mathbf{w}_i^* is the unit vector of the axis of the top revolute joint in the i th leg when the mobile platform is in its reference orientation, which is given as

$$\mathbf{w}_i^* = [-\sin\eta_i \sin\beta \ \cos\eta_i \sin\beta \ \cos\beta]^T \quad (4)$$

Let the input error of the SPMs be $\Delta\mathbf{x}$, the orientation error of the mobile platform $\Delta\boldsymbol{\varphi}$ under rigid-body motion being derived from

$$\mathbf{J}\Delta\boldsymbol{\varphi} = \Delta\mathbf{x} \quad (5)$$

where $\Delta\mathbf{x} = [\Delta\theta_1 \ \Delta\theta_2 \ \Delta\theta_3]^T$ and $\Delta\boldsymbol{\varphi} = [\Delta\varphi_x \ \Delta\varphi_y \ \Delta\varphi_z]^T$. Moreover, $\mathbf{J} = [\mathbf{j}_1 \ \mathbf{j}_2 \ \mathbf{j}_3]^T$ is the kinematic Jacobian matrix of the manipulator [11], and $\mathbf{j}_i = (\mathbf{v}_i \times \mathbf{w}_i) / (\mathbf{u}_i \times \mathbf{v}_i \cdot \mathbf{w}_i)$.

3.1. The Cartesian stiffness matrix

To model the center shift and orientation error for SPMs with flexible limbs, we need to find the overall stiffness of the manipulator structure. The virtual-spring method is adopted in this work for stiffness modeling. In this method, link flexibility is replaced by an n -dof virtual spring associated with the mobility freedoms describing both the static translational and rotational deflections and the coupling between them, where the spring compliance is calculated by means of Euler–Bernoulli beam theory. The flexibility of the single kinematic leg of the SPM in question is illustrated in Fig. 3(a), in accordance to the force diagram of Fig. 3(b) and the associated deflection and joint displacements in Fig. 3(c), the corresponding virtual springs and passive joints being described below:

- a 1-dof virtual spring representing the actuator stiffness defined by the deflection $\Delta\theta_i$;
- a 6-dof virtual spring describing the stiffness of the proximal curved link defined by the rotational deflection $\Delta\mathbf{u}_{i1} = [\Delta u_1^i, \Delta u_2^i, \Delta u_3^i]^T$ and translational deflection $\Delta\mathbf{u}_{i2} = [\Delta u_4^i, \Delta u_5^i, \Delta u_6^i]^T$;

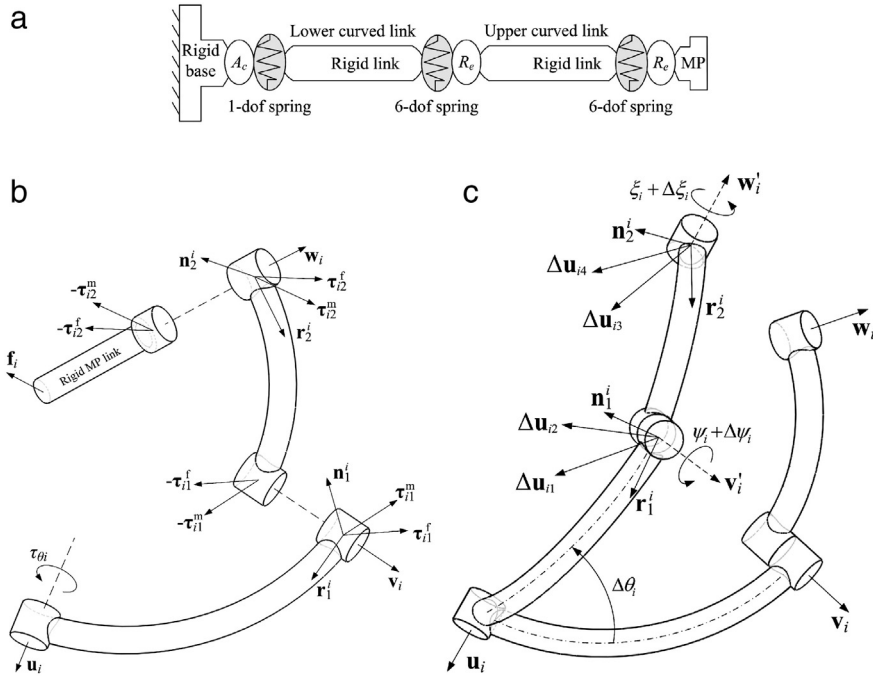


Fig. 3. Flexible model of a single limb: (a) virtual spring model, where A_c stands for the actuator, R_c for revolute joint; (b) force diagram of the i th limb, where τ^m and τ^f stand for the moments and forces in frame $r_1^i v_1^i (r_2^i w_1^i)$; (c) link deflections and joint displacements in the i th leg.

- a 1-dof passive R-joint between the two links in each leg, allowing one rotational displacement $\Delta\psi_i$;
- a 6-dof virtual spring describing the stiffness of the distal curved link defined by the rotational deflection $\Delta\mathbf{u}_{i3} = [\Delta u_{i7}^l, \Delta u_{i8}^l, \Delta u_{i9}^l]^T$ and translational deflection $\Delta\mathbf{u}_{i4} = [\Delta u_{i10}^l, \Delta u_{i11}^l, \Delta u_{i12}^l]^T$;
- a 1-dof passive R-joint between the distal curved link and the moving platform, allowing one rotational displacement $\Delta\xi_i$.

The center of the SPM, or the center of the base frame, is the designated origin of the reference frame of the mobile platform. The small-amplitude deformation screw of the MP can be expressed as:

$$\hat{\mathbf{S}}_0^i = \begin{bmatrix} \Delta\phi \\ \Delta\mathbf{p} \end{bmatrix} = \mathbf{J}_\phi^i \Delta\phi_i + \mathbf{J}_u^i \Delta\mathbf{u}_i \quad (6)$$

with

$$\mathbf{J}_\phi^i = [\hat{\mathbf{S}}_A^i \quad \hat{\mathbf{S}}_B^i \quad \hat{\mathbf{S}}_C^i], \quad \Delta\phi_i = [\Delta\theta_i \quad \Delta\psi_i \quad \Delta\xi_i]^T \quad (7a)$$

$$\mathbf{J}_u^i = [\hat{\mathbf{S}}_{u1}^i \quad \hat{\mathbf{S}}_{u2}^i \quad \dots \quad \hat{\mathbf{S}}_{u12}^i], \quad \Delta\mathbf{u}_i = [\Delta u_{i1}^l \quad \Delta u_{i2}^l \quad \dots \quad \Delta u_{i12}^l]^T \quad (7b)$$

The corresponding unit screws are expressed as

$$\begin{aligned} \hat{\mathbf{S}}_A^i &= \begin{bmatrix} \mathbf{u}_i \\ \mathbf{0} \end{bmatrix}, \quad \hat{\mathbf{S}}_B^i = \begin{bmatrix} \mathbf{v}_i \\ \mathbf{0} \end{bmatrix}, \quad \hat{\mathbf{S}}_C^i = \begin{bmatrix} \mathbf{w}_i \\ \mathbf{0} \end{bmatrix} \\ \hat{\mathbf{S}}_{u1}^i &= \begin{bmatrix} \mathbf{r}_1^i \\ \mathbf{b}_i \times \mathbf{r}_1^i \end{bmatrix}, \quad \hat{\mathbf{S}}_{u2}^i = \hat{\mathbf{S}}_B^i, \quad \hat{\mathbf{S}}_{u3}^i = \begin{bmatrix} \mathbf{n}_1^i \\ \mathbf{b}_i \times \mathbf{n}_1^i \end{bmatrix}, \quad \hat{\mathbf{S}}_{u4}^i = \begin{bmatrix} \mathbf{0} \\ \mathbf{r}_1^i \end{bmatrix}, \quad \hat{\mathbf{S}}_{u5}^i = \begin{bmatrix} \mathbf{0} \\ \mathbf{v}_i \end{bmatrix}, \quad \hat{\mathbf{S}}_{u6}^i = \begin{bmatrix} \mathbf{0} \\ \mathbf{n}_1^i \end{bmatrix} \\ \hat{\mathbf{S}}_{u7}^i &= \begin{bmatrix} \mathbf{r}_2^i \\ \mathbf{c}_i \times \mathbf{r}_2^i \end{bmatrix}, \quad \hat{\mathbf{S}}_{u8}^i = \hat{\mathbf{S}}_C^i, \quad \hat{\mathbf{S}}_{u9}^i = \begin{bmatrix} \mathbf{n}_2^i \\ \mathbf{c}_i \times \mathbf{n}_2^i \end{bmatrix}, \quad \hat{\mathbf{S}}_{u10}^i = \begin{bmatrix} \mathbf{0} \\ \mathbf{r}_2^i \end{bmatrix}, \quad \hat{\mathbf{S}}_{u11}^i = \begin{bmatrix} \mathbf{0} \\ \mathbf{w}_i \end{bmatrix}, \quad \hat{\mathbf{S}}_{u12}^i = \begin{bmatrix} \mathbf{0} \\ \mathbf{n}_2^i \end{bmatrix} \end{aligned} \quad (8)$$

with

$$\mathbf{n}_1^i = \frac{\mathbf{u}_i \times \mathbf{v}_i}{\|\mathbf{u}_i \times \mathbf{v}_i\|}, \quad \mathbf{r}_1^i = \frac{\mathbf{v}_i \times \mathbf{n}_1^i}{\|\mathbf{v}_i \times \mathbf{n}_1^i\|}; \quad \mathbf{n}_2^i = \frac{\mathbf{v}_i \times \mathbf{w}_i}{\|\mathbf{v}_i \times \mathbf{w}_i\|}, \quad \mathbf{r}_2^i = \frac{\mathbf{w}_i \times \mathbf{n}_2^i}{\|\mathbf{w}_i \times \mathbf{n}_2^i\|} \quad (9)$$

where $\Delta \mathbf{p} = [\Delta x, \Delta y, \Delta z]^T$ is the vector of positional error of the center of rotation. Moreover, \mathbf{b}_i and \mathbf{c}_i are the position vectors of points B_i and C_i , respectively. Obviously, $\Delta \mathbf{p}$ is zero when only joint displacements are considered, by virtue of the zero vectors in the lower parts of $\hat{\mathbf{S}}_A^i, \hat{\mathbf{S}}_B^i$ and $\hat{\mathbf{S}}_C^i$. This means that the joint variations due to rigid-body motions of the links have no influence on the position of the rotation center.

Eq. (6) relates the end-effector deflection to the articulated joint displacements and elastic deformations in the i th leg, which can be rewritten by separating all the variation terms into those of the passive joints and the ones due to elastic deflections and actuator compliance,

$$\mathbf{S}_O^i = \mathbf{J}_\theta^i \Delta \boldsymbol{\theta}_i + \mathbf{J}_q^i \Delta \mathbf{q}_i \quad (10)$$

with

$$\mathbf{J}_\theta^i = [\hat{\mathbf{S}}_A^i \quad \hat{\mathbf{S}}_{u1}^i \quad \dots \quad \hat{\mathbf{S}}_{u12}^i] \in \mathbb{R}^{6 \times 13}, \quad \Delta \boldsymbol{\theta}_i = [\Delta \theta_i \quad \Delta u_1^i \quad \dots \quad \Delta u_{12}^i]^T \quad (11a)$$

$$\mathbf{J}_q^i = [\hat{\mathbf{S}}_B^i \quad \hat{\mathbf{S}}_C^i] \in \mathbb{R}^{6 \times 2}, \quad \Delta \mathbf{q}_i = [\Delta \psi_i \quad \Delta \xi_i]^T \quad (11b)$$

Let the external wrench (six-dimensional array of force and moment) applied to the end of the i th leg be $\mathbf{f}_i = [\mathbf{m}_{exi}^T \quad \mathbf{f}_{exi}^T]^T$. On the other hand, in accordance to Fig. 3(b), the force/torque causing the deflection $\Delta \boldsymbol{\theta}_i$ in the i th leg being denoted by $\boldsymbol{\tau}_i = [\boldsymbol{\tau}_{\theta i}^T \quad (\boldsymbol{\tau}_{11}^i)^T \quad (\boldsymbol{\tau}_{12}^i)^T \quad (\boldsymbol{\tau}_{13}^i)^T]^T$, the equilibrium condition for the system is written as

$$\mathbf{J}_\theta^{iT} \mathbf{f}_i = \boldsymbol{\tau}_i, \quad \boldsymbol{\tau}_i = \mathbf{K}_\theta^i \Delta \boldsymbol{\theta}_i \quad (12a)$$

$$\mathbf{J}_q^{iT} \mathbf{f}_i = \mathbf{0} \quad (12b)$$

where \mathbf{K}_θ^i is the stiffness matrix in joint space. Combining Eqs. (10), (12a) and (12b), the kinetostatic model of the i th leg is reduced to

$$\begin{bmatrix} \mathbf{S}_\theta^i & \mathbf{J}_q^i \\ \mathbf{J}_q^{iT} & \mathbf{0}_{2 \times 2} \end{bmatrix} \begin{bmatrix} \mathbf{f}_i \\ \Delta \mathbf{q}_i \end{bmatrix} = \begin{bmatrix} \mathbf{S}_O^i \\ \mathbf{0}_{2 \times 1} \end{bmatrix} \quad (13)$$

where the 6×6 block $\mathbf{S}_\theta^i = \mathbf{J}_\theta^i (\mathbf{K}_\theta^i)^{-1} \mathbf{J}_\theta^{iT}$ represents the spring compliance relative to the reference frame on the moving platform, and the block \mathbf{J}_q^i takes into account the passive-joint influence on the MP motions.

Moreover, \mathbf{K}_θ^i is a 13×13 matrix, describing the stiffness of the virtual springs and the actuators, which takes the form:

$$\mathbf{K}_\theta^i = \begin{bmatrix} K_{act}^i & \mathbf{0}_{1 \times 6} & \mathbf{0}_{1 \times 6} \\ \mathbf{0}_{6 \times 1} & \mathbf{K}_{L_1}^i & \mathbf{0}_{6 \times 6} \\ \mathbf{0}_{6 \times 1} & \mathbf{0}_{6 \times 6} & \mathbf{K}_{L_2}^i \end{bmatrix} \quad (14)$$

where K_{act}^i describes the i th actuator stiffness, while $\mathbf{K}_{L_1}^i$ and $\mathbf{K}_{L_2}^i$, respectively, are the 6×6 stiffness matrices of the proximal and distal curved links in the i th leg. The compliance matrix $(\mathbf{K}_{L_{1(2)}}^i)^{-1} = \mathbf{C}_{1(2)}^i$, $i = 1, 2, 3$, of the proximal (distal) curved link can be found using Castigliano's theorem, as presented in Section 3.2.

The matrix $\mathbf{J}_\theta^i \in \mathbb{R}^{6 \times 13}$ is the Jacobian matrix associated with the virtual springs and $\mathbf{J}_q^i \in \mathbb{R}^{6 \times 2}$ the one associated with the passive joints. The Cartesian stiffness matrix \mathbf{K}_i of the i th leg is extracted from the inverse of the matrix in Eq. (13)

$$\mathbf{K}_i' = \begin{bmatrix} \mathbf{S}_\theta^i & \mathbf{J}_q^i \\ \mathbf{J}_q^{iT} & \mathbf{0}_{2 \times 2} \end{bmatrix}^{-1} \quad (15)$$

As a result, the Cartesian stiffness matrix \mathbf{K}_i mapping displacement screw to wrench is obtained as the first 6×6 block in \mathbf{K}_i' . From $\mathbf{f} = \sum_{i=1}^3 \mathbf{f}_i$, $\mathbf{S}_O = \mathbf{S}_O$ and $\mathbf{f}_i = \mathbf{K}_i \mathbf{S}_O^i$, the Cartesian stiffness matrix \mathbf{K} of the system is found by simple addition in accordance to $\mathbf{f} = \mathbf{K} \mathbf{S}_O$, namely,

$$\mathbf{K} = \sum_{i=1}^3 \mathbf{K}_i \quad (16)$$

The stiffness matrix \mathbf{K} consists of rotational, translational and coupling blocks. Liu's stiffness matrix [8], $\mathbf{K} = \mathbf{J} \mathbf{K}_{act} \mathbf{J}^T$, and Enferadi's [9] only considered the rotational block. Compared to Liu's and Enferadi's models developed through force analysis, matrix Eq. (16) can be readily used for SPM parameterization and design optimization.

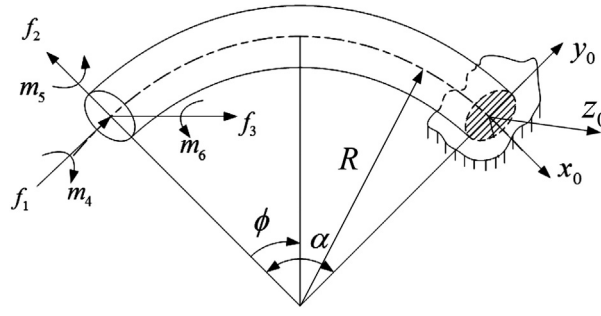


Fig. 4. A curved beam element acted upon by an external wrench.

The SPM deformation screw is found as:

$$\mathbf{S}_0 = [\Delta\boldsymbol{\varphi}^T \quad \Delta\mathbf{p}^T]^T = \mathbf{K}^{-1} \mathbf{f} \quad (17)$$

Compared to the conventional error formulation of Eq. (5), the derived error model Eq. (17) includes not only the orientational deflection but also the positional deflection as expressed by Eq. (6). The translational displacement $\Delta\mathbf{p}$ in \mathbf{S}_0 will not necessarily vanish when an external wrench is applied to the end-effector. This means that the centers of the two plates have separated. To make it clear, we denote the separation of the two centers as the *MP center shift*.

3.2. Compliance matrix formulation of curved beam

To derive the stiffness of the SPM limb, the compliance of a circular curved beam is to be formulated. A cantilever with forces and moments applied onto the free end is shown in Fig. 4, the corresponding compliance matrix \mathbf{C} being calculated by means of Euler–Bernoulli beam theory. To this end, the strain energy is expressed as

$$U = \frac{R}{2} \int_0^\alpha \left[\frac{(f'_1)^2}{EA} + \frac{(f'_2)^2}{GA} + \frac{(f'_3)^2}{GA} + \frac{(m'_4)^2}{Gl_x} + \frac{(m'_5)^2}{El_y} + \frac{(m'_6)^2}{El_z} \right] d\phi \quad (18)$$

with the forces and moments defined as

$$\begin{aligned} f'_1 &= f_1 \cos \phi - f_2 \sin \phi \\ f'_2 &= f_1 \sin \phi + f_2 \cos \phi \\ f'_3 &= f_3 \\ m'_4 &= m_4 \cos \phi - m_5 \sin \phi - f_3 R (1 - \cos \phi) \\ m'_5 &= m_4 \sin \phi + m_5 \cos \phi + f_3 R \sin \phi \\ m'_6 &= m_6 - f_1 R (1 - \cos \phi) - f_2 R \sin \phi. \end{aligned}$$

Using Castigliano's theorem [12], the deflections are obtained by differentiation of Eq. (18):

$$\Delta u_1 = \frac{\partial U}{\partial m_4}, \quad \Delta u_2 = \frac{\partial U}{\partial m_5}, \quad \Delta u_3 = \frac{\partial U}{\partial m_6}, \quad \Delta u_4 = \frac{\partial U}{\partial f_1}, \quad \Delta u_5 = \frac{\partial U}{\partial f_2}, \quad \Delta u_6 = \frac{\partial U}{\partial f_3}. \quad (19)$$

Subsequently, the relationship between the deflections and wrench is established as

$$\begin{bmatrix} \Delta u_1 \\ \Delta u_2 \\ \Delta u_3 \\ \Delta u_4 \\ \Delta u_5 \\ \Delta u_6 \end{bmatrix} = \begin{bmatrix} C_{11} & C_{12} & 0 & 0 & 0 & C_{16} \\ C_{12} & C_{22} & 0 & 0 & 0 & C_{26} \\ 0 & 0 & C_{33} & C_{34} & C_{35} & 0 \\ 0 & 0 & C_{34} & C_{44} & C_{45} & 0 \\ 0 & 0 & C_{35} & C_{45} & C_{55} & 0 \\ C_{16} & C_{26} & 0 & 0 & 0 & C_{66} \end{bmatrix} \begin{bmatrix} m_4 \\ m_5 \\ m_6 \\ f_1 \\ f_2 \\ f_3 \end{bmatrix} \quad \text{or} \quad \Delta \mathbf{u} = \mathbf{C} \mathbf{f} \quad (20)$$

The entries of the compliance matrix \mathbf{C} are given in Appendix A.

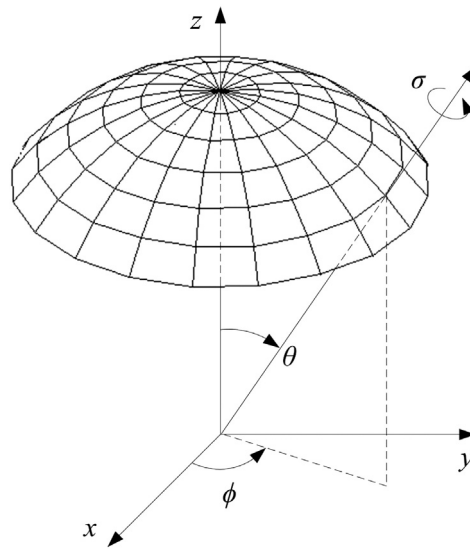


Fig. 5. Orientation representation of the azimuth-tilt-torsion angles.

4. Case studies

Henceforth, the MP orientation is represented by *azimuth-tilt-torsion* (ϕ - θ - σ) angles [13], as shown in Fig. 5, the analysis being carried out under one given working mode [14], characterized by $(\mathbf{u}_i \times \mathbf{v}_i) \cdot \mathbf{w}_i \leq 0$, $i = 1, 2, 3$. Moreover, the actuator stiffness is set to $K_{\text{act}}^i = 10^6$ Nm/rad for examples I and II.

4.1. Example I: unlimited-roll SPM

The first example pertains to an unlimited-roll SPM [15,16] shown in Fig. 6(a), that consists only of three curved links connected to the MP. The three links are driven by actuators moving independently on a circular guide. The dimensions and link parameters of the SPM, which admits a relatively large dexterous workspace [16], are listed in Table 1, where r is the radius of the circular cross section of the curved link and R is the radius of the midcurve.

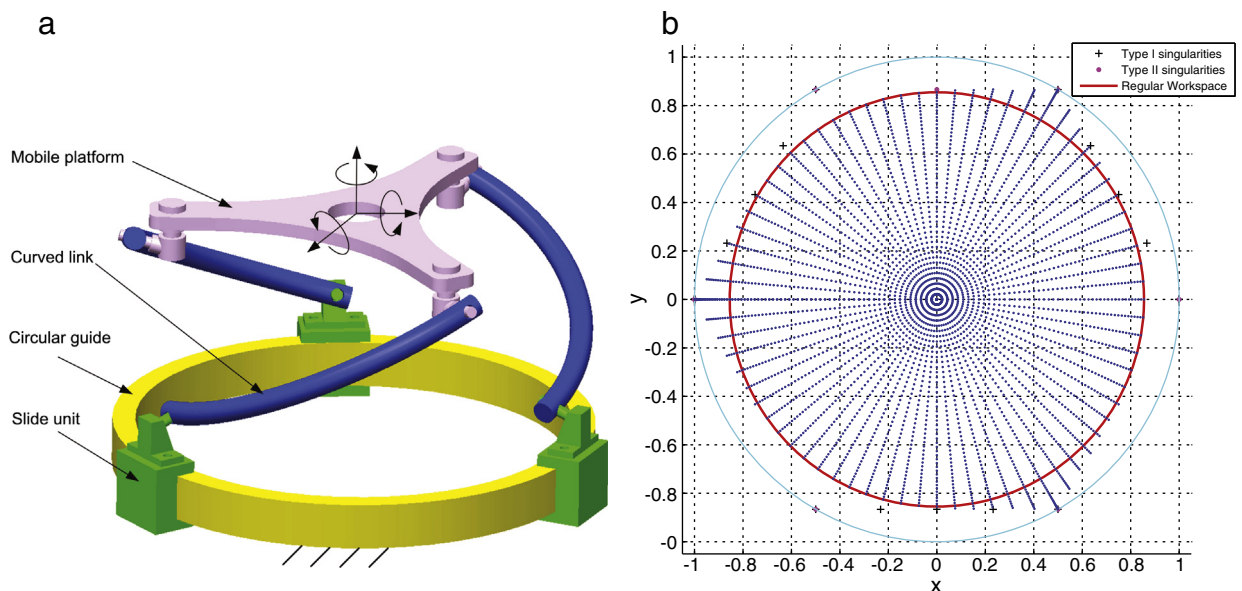


Fig. 6. A spherical parallel manipulator with unlimited roll: (a) schematic diagram; (b) its regular workspace with $\sigma = 0$.

Table 1
Dimensions and parameters of the special SPM.

SPM			Link			
a_1	a_2	β	R [m]	r [m]	E [GPa]	ν
60°	90°	90°	0.200	0.0075	210	0.3

Fig. 6(b) shows the workspace on a unit sphere projected in the xy plane for the SPM with $\sigma = 0$. Similarly, the workspace can be obtained for different values of σ . The link is made of steel of Young's modulus E , Poisson's ratio ν and shear modulus $G = E/(2 + 2\nu)$. From Eq. (20), the compliance matrix of the distal curved link is calculated as

$$\mathbf{C}_2 = \begin{bmatrix} 6.923 & -0.575 & 0 & 0 & 0 & 0.388 \\ -0.575 & 6.923 & 0 & 0 & 0 & 0.632 \\ 0 & 0 & 6.020 & -0.438 & -0.767 & 0 \\ 0 & 0 & -0.438 & 0.055 & 0.077 & 0 \\ 0 & 0 & -0.767 & 0.077 & 0.121 & 0 \\ 0.388 & 0.632 & 0 & 0 & 0 & 0.192 \end{bmatrix} \cdot 10^{-4} \quad (21)$$

The blocks corresponding to rotation, translation and coupling are given in rad/Nm, m/N and rad/N, respectively. For configurations with *tilt* angle $\theta = 0$, the stiffness matrix is constantly equal to

$$\mathbf{K} = \begin{bmatrix} \mathbf{K}_{rr} & \mathbf{K}_{rt} \\ \mathbf{K}_{rt}^T & \mathbf{K}_{tt} \end{bmatrix} = \begin{bmatrix} 0.055 & 0 & 0 & -0.373 & 0.430 & 0 \\ 0 & 0.055 & 0 & -0.430 & -0.373 & 0 \\ 0 & 0 & 0.332 & 0 & 0 & 0.745 \\ -0.373 & -0.430 & 0 & 6.233 & 0 & 0 \\ 0.430 & -0.373 & 0 & 0 & 6.233 & 0 \\ 0 & 0 & 0.745 & 0 & 0 & 1.849 \end{bmatrix} \cdot 10^6 \quad (22)$$

The entries \mathbf{K}_{rr} , \mathbf{K}_{rt} and \mathbf{K}_{tt} are given in Nm/rad, N/rad and N/m, respectively. For any applied external wrench, the deformation of the SPM can be determined. An example is given for a vector of pure moments $\mathbf{m} = [10, 10, 10]^T$ Nm, which induce the deformation screw

$$\mathbf{S}_0 = [2.985 \quad 2.985 \quad 0.314; \quad 0.385 \quad -0.028 \quad -0.127]^T$$

where the angular deflection is given hereafter within the deformation screw in μrad , which leads to $\|\Delta\phi\| = 4.232 \mu\text{rad} = 0.243^\circ$ and $\|\Delta\mathbf{p}\| = 0.406 \text{ mm}$.

The stiffness matrix Eq. (22) is obtained for curved links of uniform cross-section, as shown in Fig. 6(a). In a real design, the curved link can have embodiment of cylindrical ends, as shown in Fig. 1. For this type of links, the diagonal entries of the stiffness can slightly increase, leading to a smaller deflection.

4.1.1. SPM compliance at singular configurations

The stiffness matrix at certain configurations may become singular. Taking $[90^\circ, 60^\circ, 0]$, for example, the SPM encounters a parallel singularity, where $\det(\mathbf{A}) = 0$, as depicted in Fig. 6(b), and the stiffness matrix is

$$\mathbf{K} = \begin{bmatrix} 0.067 & 0.101 & -0.007 & -0.523 & -0.333 & 0.084 \\ 0.101 & 0.192 & 0.082 & -0.832 & -0.608 & 0.637 \\ -0.007 & 0.082 & 0.205 & -0.061 & -0.210 & 1.130 \\ -0.523 & -0.832 & -0.061 & 4.602 & 2.287 & -1.320 \\ -0.333 & -0.608 & -0.210 & 2.287 & 3.475 & -1.269 \\ 0.084 & 0.637 & 1.130 & -1.320 & -1.269 & 6.876 \end{bmatrix} \cdot 10^6 \quad (23)$$

In matrix Eq. (23), $\text{rank}(\mathbf{K}_{rr}) = 2$, the stiffness matrix thus being singular. The problem of calculating the displacements can be solved by means of least squares based on the QR decomposition [17], namely,

$$\begin{bmatrix} \mathbf{K} \\ \mathbf{a}^T \end{bmatrix} \mathbf{S}_0 = \begin{bmatrix} \mathbf{f} \\ 0 \end{bmatrix} \quad (24)$$

where \mathbf{a} is the last column of matrix \mathbf{R} from \mathbf{K} , which spans the null space of \mathbf{K} . The solution sought that lies outside the null space of \mathbf{K} . With the moment \mathbf{m} applied on the MP, the twist deflections are calculated as:

$$\mathbf{S}_0 = [11.502 \quad -4.747 \quad 4.782; \quad 0.285 \quad 0.234 \quad -0.390]^T \quad (25)$$

As \mathbf{K} is singular, the deformation screws will not be definite. By means of the least square method after spanning the null space, the deformation screws are approximated via linear regression. From kinematics, the MP generates a finite rotation about its center of rotation O at this type of singularity. Another example is the case of a serial singularity, for instance, $[45^\circ, 60^\circ, 0]$, where the stiffness matrix is invertible at this type of singularity. The displacements are found as:

$$\mathbf{S}_0 = [15.307 \quad -3.246 \quad -2.443; 0.449 \quad -0.315 \quad 0.332]^T \quad (26)$$

4.1.2. Comparison with FEA results

With the parameters in Table 1, the FE model displayed in Fig. 7 was created in Ansys/Workbench to verify the foregoing model; rib stiffeners were used to make the mobile platform rigid and two passive revolute joints in each limb were used to connect the components; while a revolute joint with torsional stiffness of 10^6 Nm/rad is used to describe the actuation stiffness. The material of the model is structural steel with the same Young's and shear modulus as shown in Table 1.

To validate the model effectively, 125 orientations of $\phi \in \mathcal{S}$, $\phi \in \mathcal{S}$, and $\theta \in \{0, 15^\circ, 30^\circ, 45^\circ, 50^\circ\}$, where $\mathcal{S} = \{0, 45^\circ, 90^\circ, 120^\circ, 180^\circ\}$, under the external moments $\mathbf{m} = [10, 10, 10]^T$ Nm, were analyzed. The corresponding translational and rotational displacements, $\|\Delta \mathbf{p}\|$ and $\|\Delta \phi\|$, are shown in Fig. 8. At configurations with tilt angle $\theta = 0$, the FE solved deflections are $\|\Delta \mathbf{p}\| = 0.401 \pm 0.0004$ mm and $\|\Delta \phi\| = 0.237 \pm 0.022^\circ$, which are quite close to the analytical solutions. Henceforth, the relative error (%) between the developed model and FE analysis results is defined as

$$Err = |\delta_{Ana} - \delta_{Fea}| / \delta_{Fea} \cdot 100\% \quad (27)$$

where δ stands for the δp or $\delta \phi$. The average relative error for $\|\Delta \mathbf{p}\|$ is 1.48% and the average difference is 0.014 mm. For $\|\Delta \phi\|$, the average difference is 0.035° or 4.17% of relative error. In contrast, the difference of the results obtained from the FEA approach and the developed model for the most workspace points is below 5%. An exception is the SPM at singular configuration. For instance, at the singular configuration of $[45^\circ, 60^\circ, 0]$ under $\mathbf{m} = [10, 10, 10]^T$ Nm, the FE solved deflections are $\|\Delta \mathbf{p}\| = 0.635$ mm and $\|\Delta \phi\| = 1.041^\circ$. Compared to the analytical solution Eq. (26), the difference for the orientation error rises up to about 13%. The comparison shows that the developed stiffness model can effectively calculate the manipulator stiffness.

In the FE model, we consider only major geometric dimensions. Details such as round corner or chamfers are not included. While such details affect the stress, they have less influence on the deflection.

4.1.3. Isocontours of MP center shift and orientation error

Fig. 9(a) and (b) illustrate the isocontours of the MP center shift and orientation error throughout the regular workspace. The maps are formulated with the maximum magnitude at each discrete point among the eight combinations of moment $\mathbf{m} = [\pm 10, \pm 10, \pm 10]^T$ Nm. It is apparent that the largest displacements occur at the workspace boundary and the three peaks of the contours appear symmetrically distributed at intervals of 120° . The maximum orientation error and center shift are 3.5° and 2 mm, respectively, for the link properties given, the MP oriented at $\phi = -70^\circ$. Within the region $\theta \leq 30^\circ$, the orientation accuracy due to the elastic deformation can reach 1° , whereas the center shift can reach up to 1.5 mm, which cannot be ignored when high positional accuracy is needed. Given the SPM symmetry, the other cases of σ -orientations generate the same isocontour maps with rotational symmetry to Fig. 9(a) and (b), respectively. It can be predicted that the global stiffness becomes weaker from the center region of the workspace to the boundary and its 3D contour map resembling a conical surface.

Fig. 9(c) displays the orientation error when only the actuation compliance is considered. By comparison to Fig. 9(b), it is seen that the limb flexibility strongly influences the orientation error. The link properties should thus be an important consideration in the SPM design.

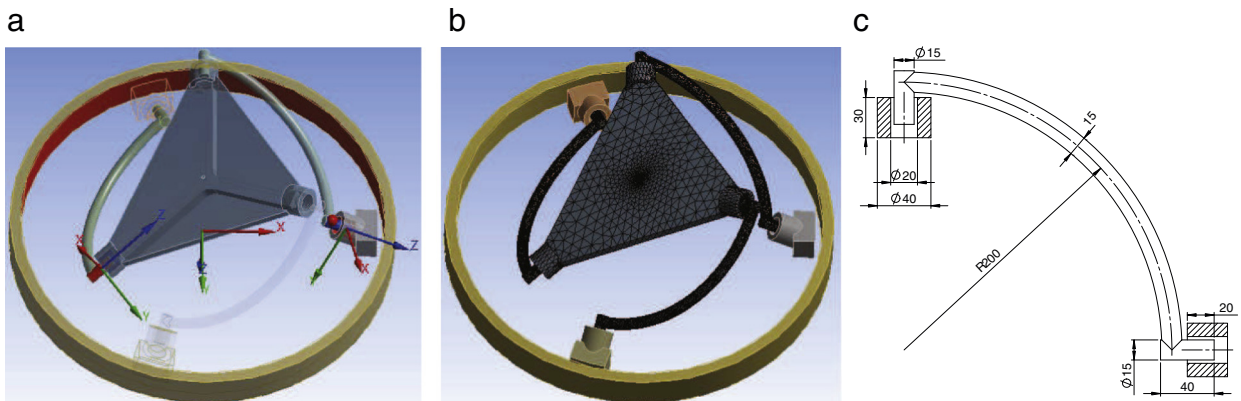


Fig. 7. SPM model for FE analysis: (a) revolute joints; (b) link meshing; (c) link detail, where bearings mounted between the shaft and the hole are not displayed.

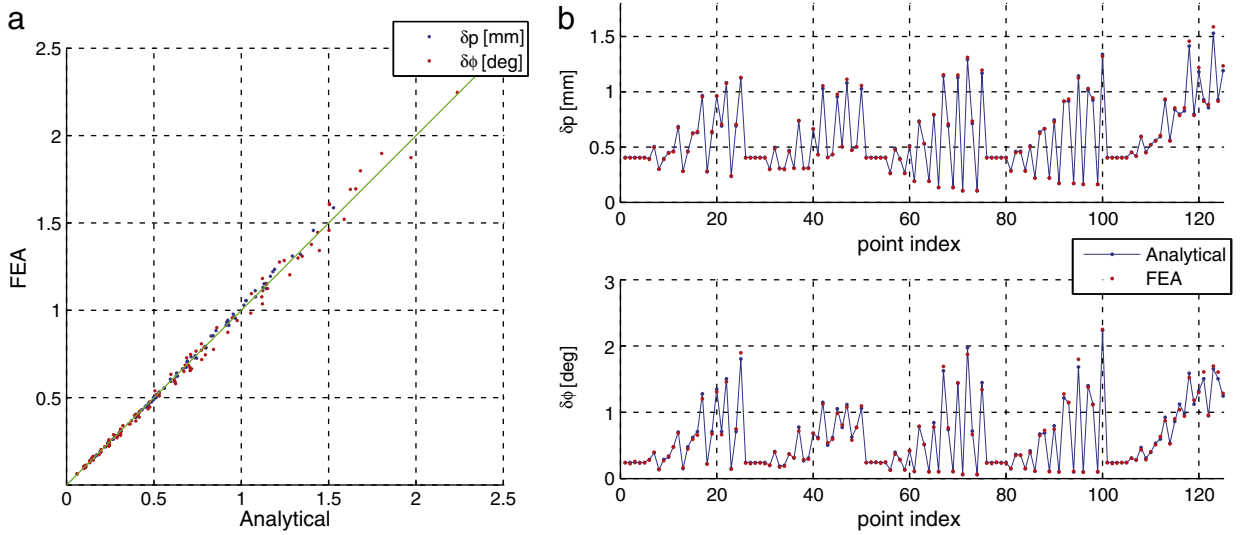


Fig. 8. Comparison of the linear and angular deflections between the FEA and analytical approaches: (a) correlations; (b) error variations, where $\delta p = \|\Delta p\|$, $\delta\phi = \|\Delta\phi\|$.

4.2. Example II: an alternative structure of a co-axial SPM

In this example, an alternative structure of the SPM in Example I, shown in Fig. 10, is studied. At the orientation $[0, 0, 0]$, the Cartesian stiffness matrix is computed as:

$$\mathbf{K} = \begin{bmatrix} 0.021 & 0 & 0 & -0.092 & 0.183 & 0 \\ 0 & 0.021 & 0 & -0.183 & -0.092 & 0 \\ 0 & 0 & 0.127 & 0 & 0 & 0.247 \\ -0.092 & -0.183 & 0 & 3.253 & 0 & 0 \\ 0.183 & -0.092 & 0 & 0 & 3.253 & 0 \\ 0 & 0 & 0.247 & 0 & 0 & 1.808 \end{bmatrix} \cdot 10^5 \quad (28)$$

Compared to matrix Eq. (22), the diagonal elements are much smaller, which imply that this SPM will generate large twist deformation under moment m :

$$\mathbf{S}_0 = [12.043 \quad 12.043 \quad 1.0647; \quad 1.019 \quad -0.336 \quad -0.146]^T$$

The isocontours for the orientation error and center shift are displayed in Fig. 11. It is seen that both the MP center shift and orientation error are larger than the SPM in Example I, which indicates that the presence of the circular guide of SPM in Fig. 6(a) effectively reduces the positioning errors.

4.3. Example III: Agile Wrist

This example borrows the geometric parameters of the Agile Wrist [18], i.e., $\alpha_1 = \alpha_2 = 90^\circ, \beta = \gamma = \sin^{-1}(\sqrt{6}/3)$, as shown in Fig. 12, whose architecture determines a large workspace with $\sigma = 30^\circ$, but keeps the same properties of the circular curved beam. The actuation stiffness is $K_{act} = 5.44 \cdot 10^5$ Nm/rad. The isocontours for the center shift and orientation error are mapped within a dexterous workspace, as seen in Fig. 13. When $\sigma = 0$, the maximum orientation error can reach up to 12° at the workspace bounds while the center shift is 4.5 mm. With *torsion* angle σ increasing, the MP center shift and orientation error become smaller.

5. Conclusions

This paper investigates the MP center shift in spherical parallel manipulators with the consideration of limb flexibility. On the basis of screw theory, the virtual-spring method, supported with Castigliano's theorem is adopted for the stiffness modeling of SPMs. The model developed is validated by means of FEA. The elastic deformation for the SPMs at singular configurations is given due attention, which is handled by means of least square method, based on the QR decomposition.

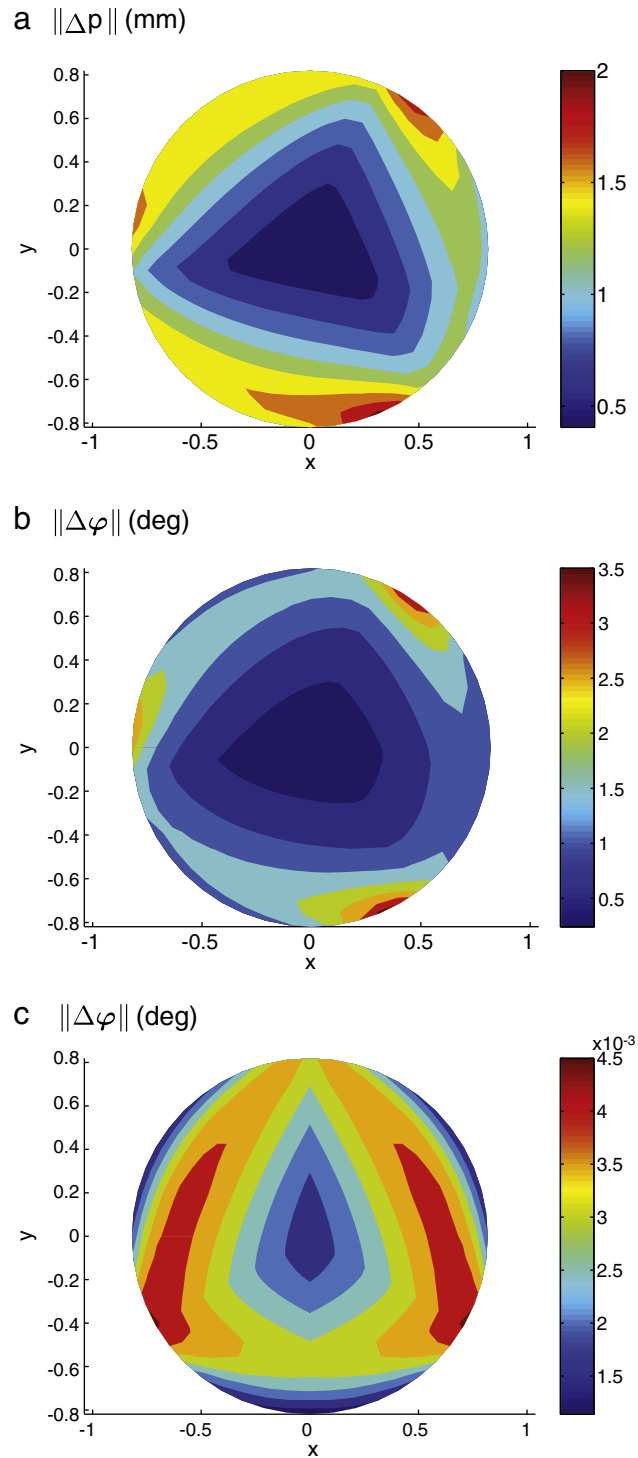


Fig. 9. MP center shift and orientation error for the unlimited-roll SPM throughout the regular workspace with orientation $\sigma = 0$: (a) and (b) both actuation and link compliance are considered; (c) only actuation compliance is considered.

A major contribution of the paper is the development of a method for qualifying the MP center shift of SPMs. The method addresses a common problem with SPMs of revolute joints. The proposed approach is illustrated with case studies of SPMs with different structures, whose isocontours for the MP center shift and orientation errors within a prescribed workspace were mapped. Moreover, the isocontours can be used for stiffness maps of SPMs. Through comparison, it is found that the SPM with the

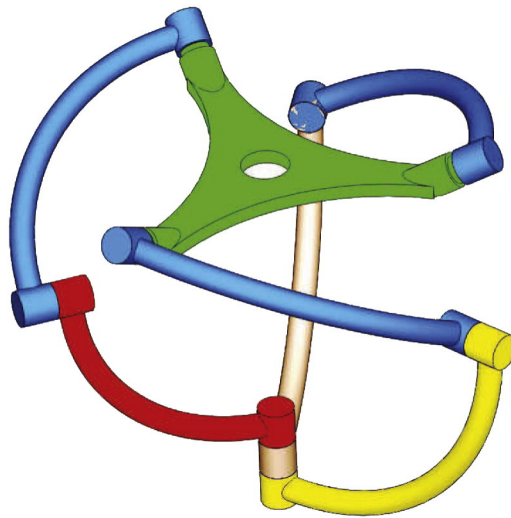


Fig. 10. An alternative structure of the unlimited-roll SPM.

circular guide yields a smaller center shift and error. The study shows that the deflection due to the limb flexibility causes large errors, in particular, the MP center shift, which could be considered in the design of SPMs, with the method developed in this work.

Supplementary data to this article can be found online at <http://dx.doi.org/10.1016/j.mechmachtheory.2014.01.001>.

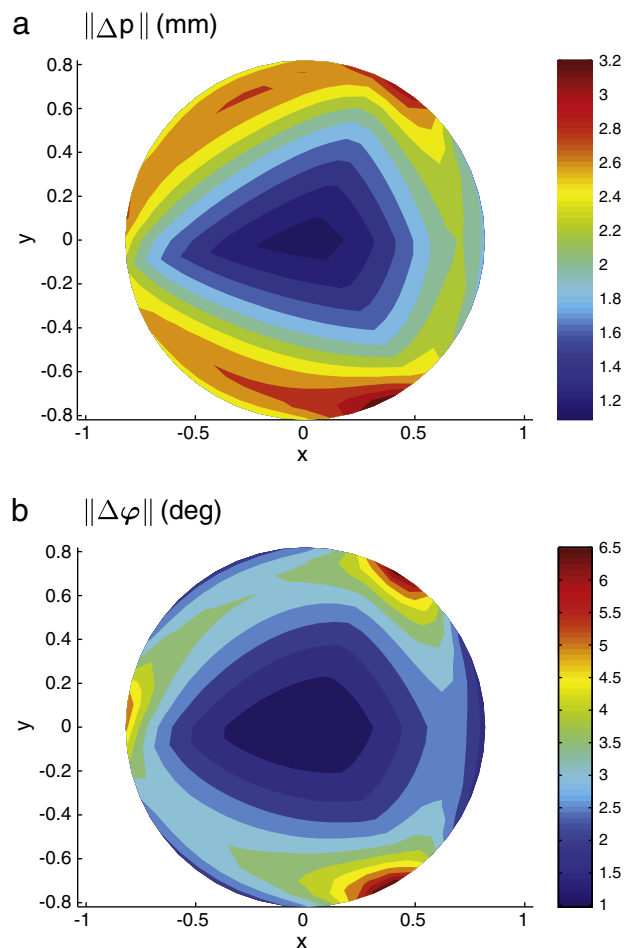


Fig. 11. MP center shift and orientation error for an alternative structure of the co-axial SPM throughout the regular workspace with orientation $\sigma = 0$.

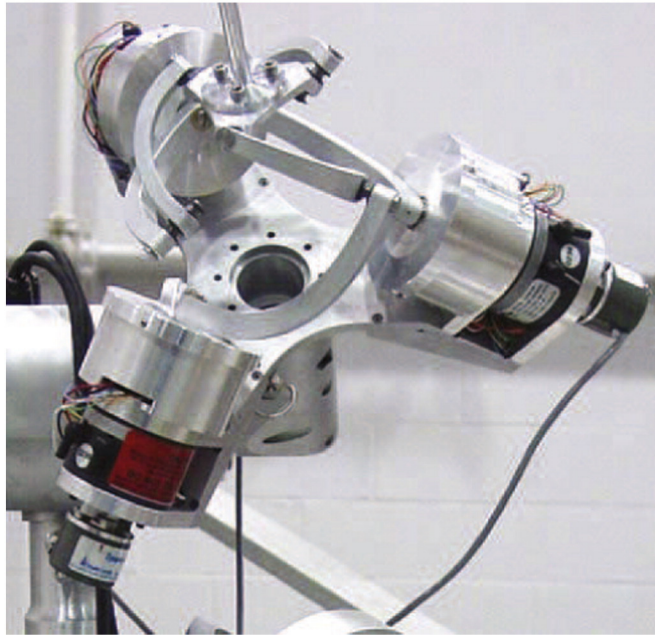


Fig. 12. Prototype of the Agile Wrist, McGill University, Canada.

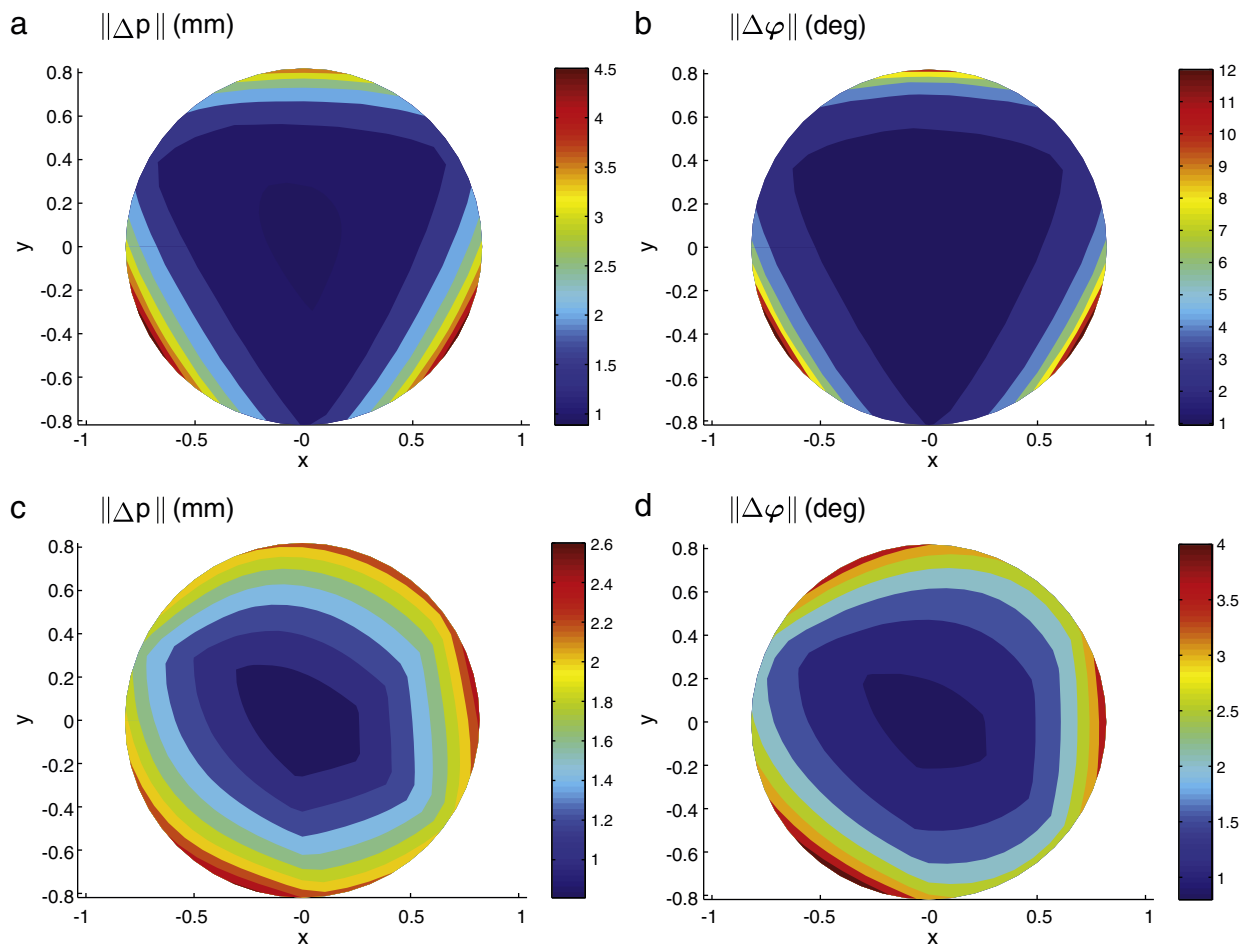


Fig. 13. MP center shift and orientation error for the Agile Wrist throughout the regular dexterous workspace with orientation: (a) and (b) $\sigma = 0$; (c) and (d) $\sigma = 30^\circ$.

Acknowledgment

The authors would like to acknowledge Professor Jorge Angeles from the Robotic Mechanical Systems Laboratory, McGill University, Canada, for his constructive advices and insightful discussion.

Appendix A

The elements of the compliance matrix of the curved beam in Eq. (20) are given as:

$$C_{11} = \frac{R}{2} \left(\frac{s_1}{GI_x} + \frac{s_2}{EI_y} \right) \quad (\text{A-1a})$$

$$C_{12} = \frac{s_8 R}{2} \left(\frac{1}{GI_x} - \frac{1}{EI_y} \right) \quad (\text{A-1b})$$

$$C_{16} = \frac{R^2}{2} \left(\frac{s_2}{EI_y} - \frac{s_7}{GI_x} \right) \quad (\text{A-1c})$$

$$C_{22} = \frac{R}{2} \left(\frac{s_2}{GI_x} + \frac{s_1}{EI_y} \right) \quad (\text{A-1d})$$

$$C_{26} = \frac{R^2}{2} \left(\frac{s_4}{GI_x} - \frac{s_2}{EI_y} \right) \quad (\text{A-1e})$$

$$C_{33} = \frac{R\alpha}{EI_z} \quad (\text{A-1f})$$

$$C_{34} = \frac{s_5 R^2}{EI_z} \quad (\text{A-1g})$$

$$C_{35} = \frac{s_6 R^2}{EI_z} \quad (\text{A-1h})$$

$$C_{44} = \frac{R}{2A} \left(\frac{s_1}{E} + \frac{s_2}{G} \right) + \frac{s_3 R^3}{2EI_z} \quad (\text{A-1i})$$

$$C_{45} = \frac{s_8 R}{2A} \left(\frac{1}{E} - \frac{1}{G} \right) + \frac{s_4 R^3}{2EI_z} \quad (\text{A-1j})$$

$$C_{55} = \frac{R}{2A} \left(\frac{s_1}{G} + \frac{s_2}{E} \right) + \frac{s_2 R^3}{2EI_z} \quad (\text{A-1k})$$

$$C_{66} = \frac{R\alpha}{GA} + \frac{R^3}{2} \left(\frac{s_3}{GI_x} + \frac{s_2}{EI_y} \right) \quad (\text{A-1l})$$

where A is the area of the beam cross section, I_x , I_y and I_z are the moments of inertia. Moreover,

$$s_1 = \alpha + \sin \alpha \cos \alpha \quad (\text{A-2a})$$

$$s_2 = \alpha - \sin \alpha \cos \alpha \quad (\text{A-2b})$$

$$s_3 = 3\alpha + \sin \alpha \cos \alpha / 2 - 4 \sin \alpha \quad (\text{A-2c})$$

$$s_4 = 1 - \cos \alpha - \sin^2 \alpha / 2 \quad (\text{A-2d})$$

$$s_5 = \sin \alpha - \alpha \quad (\text{A-2e})$$

$$s_6 = \cos \alpha - 1 \quad (\text{A-2f})$$

$$s_7 = 2 \sin \alpha - \alpha - \sin \alpha \cos \alpha \quad (\text{A-2g})$$

$$s_8 = -\sin^2 \alpha. \quad (\text{A-2h})$$

References

- [1] C.M. Gosselin, J.-F. Hamel, The Agile Eye: a high-performance three-degree-of-freedom camera-orienting device, *IEEE Int. Conf. Robot. Autom.* 1 (1994) 781–786, <http://dx.doi.org/10.1109/ROBOT.1994.351393>.
- [2] C. Gosselin, Stiffness mapping for parallel manipulators, *IEEE Trans. Robot. Autom.* 6 (3) (1990) 377–382, <http://dx.doi.org/10.1109/70.56657>.
- [3] S.-F. Chen, I. Kao, Conservative congruence transformation for joint and Cartesian stiffness matrices of robotic hands and fingers, *Int. J. Robot. Res.* 19 (2000) 835–847, <http://dx.doi.org/10.1177/02783640022067201>.
- [4] C.M. Gosselin, D. Zhang, Stiffness analysis of parallel mechanisms using a lumped model, *Int. J. Robot. Autom.* 17 (1) (2003) 17–27.
- [5] F. Majou, C. Gosselin, P. Wenger, D. Chablat, Parametric stiffness analysis of the orthoglide, *Mech. Mach. Theory* 42 (3) (2007) 296–311, <http://dx.doi.org/10.1016/j.mechmachtheory.2006.03.018>.
- [6] C. Quennouelle, C.M. Gosselin, Stiffness matrix of compliant parallel mechanisms, in: J. Lenarčič, P. Wenger (Eds.), *Advances in Robot Kinematics: Analysis and Design*, Springer, Netherlands, 2008, pp. 331–341, http://dx.doi.org/10.1007/978-1-4020-8600-7_35.
- [7] A. Pashkevich, D. Chablat, P. Wenger, Stiffness analysis of overconstrained parallel manipulators, *Mech. Mach. Theory* 44 (5) (2009) 966–982, <http://dx.doi.org/10.1016/j.mechmachtheory.2008.05.017>.
- [8] X.J. Liu, Z.L. Jin, F. Gao, Optimum design of 3-DOF spherical parallel manipulators with respect to the conditioning and stiffness indices, *Mech. Mach. Theory* 35 (9) (2000) 1257–1267, [http://dx.doi.org/10.1016/S0094-114X\(99\)00072-5](http://dx.doi.org/10.1016/S0094-114X(99)00072-5).
- [9] J. Enferadi, A.A. Tootoonchi, Accuracy and stiffness analysis of a 3-RRP spherical parallel manipulator, *Robotica* 29 (2) (2011) 193–209, <http://dx.doi.org/10.1017/S0263574710000032>.
- [10] H. Asada, J. Granito, Kinematic and static characterization of wrist joints and their optimal design, *IEEE Int. Conf. Robot. Autom.* 2 (1985) 244–250, <http://dx.doi.org/10.1109/ROBOT.1985.1087324>.
- [11] C.M. Gosselin, E. Lavoie, On the kinematic design of spherical three-degree-of-freedom parallel manipulators, *Int. J. Robot. Res.* 12 (4) (1993) 394–402, <http://dx.doi.org/10.1177/027836499301200406>.
- [12] R.C. Hibbeler, *Mechanics of Materials*, Pearson Prentice Hall, 2011.
- [13] I.A. Bonev, Direct kinematics of zero-torsion parallel mechanisms, *International Conference on Robotics and Automation, IEEE*, 2008, pp. 3851–3856, <http://dx.doi.org/10.1109/ROBOT.2008.4543802>, (Pasadena, California, USA).
- [14] I.A. Bonev, D. Chablat, P. Wenger, Working and assembly modes of the Agile eye, *International Conference on Robotics and Automation*, 2006, pp. 2317–2322, <http://dx.doi.org/10.1109/ROBOT.2006.1642048>.
- [15] S. Bai, M.R. Hansen, T.O. Andersen, Modelling of a special class of spherical parallel manipulators with Euler parameters, *Robotica* 27 (2) (2009) 161–170, <http://dx.doi.org/10.1017/S0263574708004402>.
- [16] S. Bai, Optimum design of spherical parallel manipulators for a prescribed workspace, *Mech. Mach. Theory* 45 (2) (2010) 200–211, <http://dx.doi.org/10.1016/j.mechmachtheory.2009.06.007>.
- [17] G.H. Golub, C.F. Van Loan, *Matrix Computations*, 3rd ed. Johns Hopkins University Press, Baltimore, MD, USA, 1996.
- [18] F. Bidault, C.-P. Teng, J. Angeles, Structural optimization of a spherical parallel manipulator using a two-level approach, *Proc. ASME 2001 Design Engineering Technical Conferences, DETC2001/DAC-21030*, Pittsburgh, Pennsylvania, 2001.